Published in final edited form as:
Cell Rep. 2014 September 25; 8(6): 1752–1766. doi:10.1016/j.celrep.2014.08.023.

Enhanced TLR-MYD88 Signaling Stimulates Autoinflammation in SH3BP2 Cherubism Mice and Defines the Etiology of Cherubism

Teruhito Yoshitaka[1], **Tomoyuki Mukai**[1], **Mizuho Kittaka**[1], **Lisa M. Alford**[1], **Salome Masrani**[1], **Shu Ishida**[1,2], **Ken Yamaguchi**[3], **Motohiko Yamada**[3], **Noriyoshi Mizuno**[1,2], **Bjorn R. Olsen**[4], **Ernst J. Reichenberger**[5], and **Yasuyoshi Ueki**[1]

[1]Department of Oral and Craniofacial Sciences, School of Dentistry, University of Missouri-Kansas City, MO 64108, USA

[2]Department of Periodontal Medicine, Division of Applied Life Science, Institute of Biomedical & Health Sciences, Hiroshima University, Hiroshima 734, JAPAN

[3]Department of Molecular Biology and Biochemistry, Okayama University Graduate School of Medicine, Dentistry and Pharmaceutical Sciences, Okayama 700, JAPAN

[4]Department of Developmental Biology, Harvard School of Dental Medicine, Boston, MA 02115, USA

[5]Department of Reconstructive Sciences, School of Dental Medicine, University of Connecticut Health Center, Farmington, CT 06030, USA

Summary

Cherubism is caused by mutations in SH3BP2. Studies of cherubism mice showed that TNF-α-dependent autoinflammation is a major cause for the disorder, but failed to explain why human cherubism lesions are restricted to jaws and regress after puberty. We demonstrate that the inflammation in cherubism mice is MYD88-dependent and is rescued in the absence of TLR2 and TLR4. However, germ-free cherubism mice also develop inflammation. Mutant macrophages are hyper-responsive to PAMPs (pathogen-associated molecular patterns) and DAMPs (damage-associated molecular patterns) that activate TLRs, resulting in TNF-α overproduction. Phosphorylation of SH3BP2 at Y183 is critical for the TNF-α production. Finally, SYK depletion in macrophages prevents the inflammation. These data suggest that the presence of a large amount of TLR ligands, presumably oral bacteria and DAMPs during jawbone remodeling, may cause the

Corresponding Author: Yasuyoshi Ueki, M.D., Ph.D., Department of Oral and Craniofacial Sciences, University of Missouri-Kansas City, School of Dentistry, 650 E 25th Street, Kansas City, Missouri 64108, USA, TEL: +1-816-235-5824, Fax: +1-816-235-5524, uekiy@umkc.edu.

Author contributions

Study design: TY, TM, EJR, BRO, and YU. Study conduct and data collection and analysis: TY, TM, MK, LMA, SM, SI, KY, MY, NM, and YU. Data interpretation: TY, TM, MK, EJR, BRO, and YU. YU supervised the overall study and wrote the final manuscript. All authors read the manuscript and discussed the results.

All authors state that they have no conflict of interest.

jaw-specific development of human cherubism lesions. Reduced levels of DAMPs after stabilization of jaw remodeling may contribute to the age-dependent regression.

Introduction

Autoinflammatory diseases characterized by seemingly unprovoked episodes of inflammation are caused by the pathologic activation of the innate immune system, and are defined by the lack of involvement of the acquired immune system (Masters et al., 2009; Park et al., 2012). Gene mutations responsible for rare human autoinflammatory disorders have revealed key regulators and underlying molecular mechanisms for innate immune responses (Park et al., 2012). Cherubism (OMIM#118400) is a rare genetic disorder in children characterized by disfiguring bilateral expansion of the lower face due to bone loss in the jaws and proliferation of inflammatory/fibrous lesions that often regress after puberty. Heterozygous mutations in the signaling adaptor protein SH3-domain binding protein 2 (SH3BP2) are responsible for the disorder (Ueki et al., 2001). SH3BP2, originally discovered as a protein that binds to ABL (Ren et al., 1993), has been found to interact with a variety of proteins including SYK (Deckert et al., 1998), VAV (Foucault et al., 2005), PLCγ1 and PLCγ2 (Deckert et al., 1998; Jevremovic et al., 2001), and SRC (Levaot et al., 2011a) in various cells. Phosphorylation of tyrosine residues in SH3BP2 by SYK modulates downstream signaling pathways (Maeno et al., 2003). Studies of the SH3BP2 P416R knock-in (KI, equivalent to the P418R mutation in cherubism patients) cherubism mice have shown that homozygous mutants (*Sh3bp2*$^{KI/KI}$) are a model for cherubism and that they exhibit spontaneous systemic macrophage inflammation independently of T and B cells (Ueki et al., 2007), indicating that cherubism is an autoinflammatory disease (Ferguson and El-Shanti, 2007; Masters et al., 2009). Unlike in human cherubism, lesions in *Sh3bp2*$^{KI/KI}$ mice do not regress with age. Evidence for a key role of TNF-α in inflammation in cherubism mice was provided by the finding that TNF-α-deficient *Sh3bp2*$^{KI/KI}$ mice show a significant rescue from inflammation (Ueki et al., 2007). Recently, it has been shown that SH3BP2 is a substrate of TANKYRASE and that the cherubism mutation, which is located in the TANKYRASE interaction site, results in reduced ADP-ribosylation of mutant SH3BP2, thereby decreasing its proteasomal degradation and leading to TNF-α overproduction in macrophages (Guettler et al., 2011; Levaot et al., 2011b).

Signals from toll-like receptors (TLRs) play a major role in the production of inflammatory cytokines (Mogensen, 2009; Takeuchi et al., 1999). TLRs primarily recognize conserved structures in microorganisms, known as pathogen-associated molecular patterns (PAMPs), and are activated in the mechanisms of host defense (Kawai and Akira, 2010). In addition, recent studies have demonstrated that TLRs also recognize endogenous molecules, known as damage-associated molecular patterns (DAMPs), that are released from damaged tissues or from dead or stressed cells, suggesting that TLRs can be self-activated when sterile inflammation occurs (Chen and Nunez, 2010; Kono and Rock, 2008; Zhang and Mosser, 2008). Myeloid differentiation factor-88 (MYD88) is the pivotal adaptor protein that binds to all TLRs (except for TLR3) through a toll/interleukin-1 receptor (TIR) domain, transducing TLRs signals to activate downstream transcription factors such as nuclear factor-κB (NF-κB). MYD88-deficient mice show lack of responses to PAMPs that stimulate

TLRs, indicating that the TLR-MYD88 pathway is essential for host defense (O'Neill and Bowie, 2007).

While progress has been made in understanding the function of SH3BP2 and the pathogenesis of cherubism, it is not known how SH3BP2 mutations cause excessive bone resorption and soft tissue proliferation that is primarily restricted to the jaws, and why cherubism lesions regress after puberty (Berendsen and Olsen, 2011). Here, we present data offering an explanation for the jaw- and age-associated development of autoinflammation in cherubism by elucidating mechanisms by which mutant SH3BP2 activates the MYD88-mediated pathway in macrophages in response to TLR2 and TLR4 stimulation.

Results

MYD88 ablation rescues *Sh3bp2*$^{KI/KI}$ cherubism mice from inflammation and bone loss

We hypothesized that response to oral bacteria triggering increased TLR-MYD88 pathway activation in macrophages carrying a cherubism mutation could be the main cause for the development of jaw-restricted cherubism lesions in humans. TLRs recognize bacterial pathogens by binding to their cell wall components such as peptidoglycan and lipopolysaccharides (LPS) (Akira et al., 2006), downstream of which MYD88 is critically involved in transducing signals that lead to the production of inflammatory cytokines. Indeed, MYD88-deficient mice show unresponsiveness to bacteria (O'Neill and Bowie, 2007). To investigate the effect of TLR-mediated recognition of bacterial components on the development of inflammation in *Sh3bp2*$^{KI/KI}$ mice, MYD88-deficient homozygous cherubism mice (*Sh3bp2*$^{KI/KI}$/*Myd88*$^{-/-}$) were generated. Facial swelling with eyelid closure due to skin inflammation, which is typically seen in *Sh3bp2*$^{KI/KI}$ mice by 6 weeks of age, was not observed in 10-week-old *Sh3bp2*$^{KI/KI}$/*Myd88*$^{-/-}$mice (Figure 1A). Macrophage-rich inflammatory infiltrates in lung, liver, and stomach as well as in lymph nodes were almost undetectable in tissue sections from *Sh3bp2*$^{KI/KI}$/*Myd88*$^{-/-}$mice (Figure 1B). MicroCT images of calvarial bone revealed a reduction in the number of bone erosion pits in *Sh3bp2*$^{KI/KI}$/*Myd88*$^{-/-}$mice (Figure 1C). Histomorphometric analysis of liver tissues confirmed a significant rescue from lesions in *Sh3bp2*$^{KI/KI}$/*Myd88*$^{-/-}$mice (Figure 1D). Quantitative microCT analysis of calvarial bone showed a great reduction in bone erosion in *Sh3bp2*$^{KI/KI}$/*Myd88*$^{-/-}$mice to a level comparable to that of wild-type (*Sh3bp2*$^{+/+}$) mice (Figure 1E). Consistent with the significant rescue of inflammatory lesions, serum TNF-α was undetectable in the majority of double mutants (Figure 1F). These results indicate that the MYD88-mediated signaling pathway is critically important for the development of inflammation in *Sh3bp2*$^{KI/KI}$ mice. While SH3BP2 mutation enhances RANKL-induced osteoclastogenesis (Ueki et al., 2007), lack of MYD88 did not affect the enhanced osteoclastogenesis (Figure S1). This suggests that the reduction of calvarial bone erosion in *Sh3bp2*$^{KI/KI}$/*Myd88*$^{-/-}$mice is primarily attributed to the decreased bone resorption associated with inflammation.

MYD88-mediated signaling pathway in hematopoietic cells is critical for the development of inflammation in *Sh3bp2*$^{KI/KI}$ mice

Because hematopoietic cells are responsible for inflammation in *Sh3bp2*$^{KI/KI}$ mice (Ueki et al., 2007), rescue of inflammation in *Sh3bp2*$^{KI/KI}$/*Myd88*$^{-/-}$mice suggested that the activation of the MYD88-mediated pathway in hematopoietic cells is critical for the development of inflammation. However, since MYD88 is expressed in a variety of non-hematopoietic cells such as fibroblasts (Akira et al., 2006), we investigated whether the activation of MYD88-mediated signals in non-hematopoietic cells contributes to the inflammation in *Sh3bp2*$^{KI/KI}$ mice by generating bone marrow (BM) chimeric mice. Wild-type recipient mice (*Sh3bp2*$^{+/+}$/*Myd88*$^{+/+}$, grey boxes in Figure 2A) transplanted with BM cells from *Sh3bp2*$^{KI/KI}$/*Myd88*$^{-/-}$double mutants (red box) did not develop the typical facial swelling (Figure 2A) and exhibited significantly reduced liver lesions and calvarial bone erosion (Figure 2A) compared to *Sh3bp2*$^{+/+}$/*Myd88*$^{+/+}$ mice transplanted with *Sh3bp2*$^{KI/KI}$/*Myd88*$^{+/+}$ BM cells (yellow boxes). In contrast, *Sh3bp2*$^{+/+}$/*Myd88*$^{-/-}$recipient mice (green box) transplanted with *Sh3bp2*$^{KI/KI}$/*Myd88*$^{+/+}$ BM cells exhibited facial swelling (Figure 2A) and developed liver inflammation and calvarial bone loss comparable to those in *Sh3bp2*$^{+/+}$/*Myd88*$^{+/+}$mice transplanted with *Sh3bp2*$^{KI/KI}$/*Myd88*$^{+/+}$ BM cells (Figure 2A). Quantitative analysis confirmed the above results (Figure 2B, top and middle). Serum TNF-α levels were nearly undetectable in *Sh3bp2*$^{+/+}$/*Myd88*$^{+/+}$ mice transplanted with *Sh3bp2*$^{KI/KI}$/*Myd88*$^{-/-}$cells, while they were elevated in *Sh3bp2*$^{+/+}$/*Myd88*$^{-/-}$mice transplanted with *Sh3bp2*$^{KI/KI}$/*Myd88*$^{+/+}$ cells, which were comparable to TNF-α levels in *Sh3bp2*$^{+/+}$/*Myd88*$^{+/+}$ mice transplanted with *Sh3bp2*$^{KI/KI}$/*Myd88*$^{+/+}$ cells (Figure 2B, bottom). Previously, we demonstrated that the development of macrophage-rich inflammation in *Sh3bp2*$^{KI/KI}$ mice is independent of T and B cells, but is partially dependent on macrophage colony stimulating factor (M-CSF) (Ueki et al., 2007). Taken together, these results suggest that the MYD88-mediated pathway in hematopoietic cells (primarily in macrophages) is responsible for the development of inflammation in *Sh3bp2*$^{KI/KI}$ mice and that the contribution of the pathway in non-hematopoietic cells is minimal.

TLR2 and TLR4 play a major role in the development of inflammation in cherubism mice

Significant rescue from inflammation in *Sh3bp2*$^{KI/KI}$/*Myd88*$^{-/-}$mice is consistent with our initial hypothesis that dysregulation of immune response to bacteria is primarily responsible for the inflammation in cherubism. A host recognizes pathogenic and commensal bacteria mainly through the TLR2 and TLR4 recognition of bacterial components such as peptidoglycan or LPS, respectively. To examine whether ablation of bacterial recognition via TLR2 and TLR4 rescues the inflammatory phenotype, we next knocked out both *Tlr2* and *Tlr4* genes in the *Sh3bp2*$^{KI/KI}$ mice. Strikingly, *Sh3bp2*$^{KI/KI}$/*Tlr2*$^{-/-}$/*Tlr4*$^{lps\text{-}del/lps\text{-}del}$ mice displayed rescue from facial swelling and inflammation in liver and stomach as well as reduced bone loss in calvariae (Figure 3A, center panels) compared to *Sh3bp2*$^{KI/KI}$ mice (Figure 1A–C center panels). These results were confirmed by quantitative measurements of liver inflammation and calvarial bone erosion (Figure 3B). Consistent with the phenotypic rescue, serum TNF-α levels were significantly decreased in *Sh3bp2*$^{KI/KI}$/*Tlr2*$^{-/-}$/*Tlr4*$^{lps\text{-}del/lps\text{-}del}$ triple mutants compared to *Sh3bp2*$^{KI/KI}$ mice (Figure 3C), suggesting that ligands for TLR2 and TLR4 are the major inducers of inflammation in cherubism mice.

MYD88 also serves as an adaptor protein downstream of interleukin-1 receptors (IL-1Rs) (Adachi et al., 1998). This prompted us to examine whether an IL-1R-mediated pathway may contribute to the inflammation in *Sh3bp2*$^{KI/KI}$ mice. *Sh3bp2*$^{KI/KI}$/*Il1r1*$^{-/-}$mice did exhibit facial swelling, liver and stomach inflammation, and failed to show a reduction in calvarial bone erosion (Figure 3A, left panels). Quantitative analysis revealed that IL-1R1 deficiency resulted in a partial reduction of liver inflammation but no reduction of bone erosion in calvariae (Figure 3B). Serum TNF-α levels in *Sh3bp2*$^{KI/KI}$/*Il1r1*$^{-/-}$mice were comparable to those in *Sh3bp2*$^{KI/KI}$ mice (Figure 3C). We further generated and analyzed quadruple mutant mice in which IL-1R1, TLR2, and TLR4 were ablated in the *Sh3bp2*$^{KI/KI}$ background (*Sh3bp2*$^{KI/KI}$/*Il1r1*$^{-/-}$/*Tlr2*$^{-/-}$/*Tlr4*$^{lps\text{-}del/lps\text{-}del}$) (Figure 3A, right panels). These mice exhibited rescued liver inflammation and calvarial bone erosion equivalent to *Sh3bp2*$^{KI/KI}$/*Tlr2*$^{-/-}$/*Tlr4*$^{lps\text{-}del/lps\text{-}del}$ triple mutants (Figure 3B). Serum TNF-α levels in *Sh3bp2*$^{KI/KI}$/*Il1r1*$^{-/-}$/*Tlr2*$^{-/-}$/*Tlr4*$^{lps\text{-}del/lps\text{-}del}$ quadruple mutants were comparable to those of *Sh3bp2*$^{KI/KI}$/*Tlr2*$^{-/-}$/*Tlr4*$^{lps\text{-}del/lps\text{-}del}$ triple mutants (Figure 3C). The additional benefit from IL-1R1 deficiency was a decrease in the percentage of inflamed lymph nodes from 94.4% (119/126) in *Sh3bp2*$^{KI/KI}$/*Tlr2*$^{-/-}$/*Tlr4*$^{lps\text{-}del/lps\text{-}del}$ triple mutants to 67.2% (45/67) in *Sh3bp2*$^{KI/KI}$/*Il1r1*$^{-/-}$/*Tlr2*$^{-/-}$/*Tlr4*$^{lps\text{-}del/lps\text{-}del}$ quadruple mutants (data not shown). Collectively, these results suggest that TLR2 and TLR4 activation in macrophages is the major cause of inflammation in *Sh3bp2*$^{KI/KI}$ mice and that the contribution of an IL-1R-mediated pathway to the inflammation in cherubism mice is minor compared to that of TLR2 and TLR4.

Mutant macrophages exhibit increased responsiveness to PAMP ligands for TLRs

Next, we examined whether bone marrow-derived M-CSF-dependent macrophages (BMMs) from *Sh3bp2*$^{KI/KI}$ mice have altered responsiveness to components of pathogenic microorganisms that activate TLRs. TNF-α levels in culture supernatants of *Sh3bp2*$^{KI/KI}$ BMMs stimulated with Pam3CSK4, FSL-1, heat-killed *Porphyromonas gingivalis* (HKPG) and *Listeria monocytogenes* (HKLM), Poly(I:C), LPS, ssRNA, ODN1826, which are ligands for TLR1/2, TLR2/6, TLR2, TLR3, TLR4, TLR7, and TLR9, respectively, were measured and compared to those of *Sh3bp2*$^{+/+}$ BMMs. *Sh3bp2*$^{KI/KI}$ BMMs produced increased amounts of TNF-α in response not only to TLR2 and TLR4 ligands but also to ligands that bind to other TLRs when compared to *Sh3bp2*$^{+/+}$ BMM cultures (Figure 4A–H). Heterozygous *Sh3bp2*$^{KI/+}$ BMMs were susceptible to some of the TLR ligands tested. Interestingly, TNF-α production of SH3BP2-deficient (*Sh3bp2*$^{-/-}$) BMMs in response to TLR ligands was equivalent to that of *Sh3bp2*$^{+/+}$ BMMs, indicating that lack of SH3BP2 does not reduce the macrophage responsiveness to TLR ligands *in vitro* and that SH3BP2 can modulate the sensitivity of TLRs only towards the enhancement of TNF-α production in BMMs. Further quantitative PCR analysis revealed that TLR2 or TLR4 stimulation increased TNF-α expression in *Sh3bp2*$^{KI/KI}$ BMMs at the transcriptional level (Figure 4I).

Mutant SH3BP2 increases TNF-α production through SYK-mediated activation of NF-κB

To identify molecular mechanisms that underlie the increased TNF-α production in *Sh3bp2*$^{KI/KI}$ BMMs, we examined the effect of inhibitors that selectively block signaling pathways downstream of TLRs. Because of the dominant role of TLR2/4 in *Sh3bp2*$^{KI/KI}$ mice (Figure 3A–C), we used Pam3CSK4 and LPS for further mechanistic analysis of

signaling pathways. BMMs were stimulated with Pam3CSK4 or LPS for 24 hours in the presence or absence of chemical inhibitors and TNF-α levels in the culture supernatants were measured. Among inhibitors tested (Figure S2), BMS-345541, an inhibitor of IκB kinases (IKKs) and BAY-613606, an inhibitor of SYK, showed differences in dose-dependent reduction of TNF-α levels in *Sh3bp2*$^{KI/KI}$ and *Sh3bp2*$^{+/+}$ BMM cultures (Figure 5A), suggesting that NF-κB and SYK-mediated pathways are selectively involved in *Sh3bp2*$^{KI/KI}$-specific BMM activation following TLR2 and TLR4 stimulation.

Phosphorylation levels of IKKα and IKKβ were constitutively elevated in *Sh3bp2*$^{KI/KI}$ BMMs compared to *Sh3bp2*$^{+/+}$ BMMs (Figure 5B, 0 minute). In addition, mutant cells showed sustained phosphorylation of IKKβ until 240 minutes following Pam3CSK4 and LPS stimulation, while IKKβ phosphorylation in wild-type BMMs decreased by 120 minutes. Consistent with increased activation of the canonical NF-κB pathway in *Sh3bp2*$^{KI/KI}$ BMMs, levels of IκBα were decreased throughout the culture period compared to *Sh3bp2*$^{+/+}$ BMMs (Figure 5B). In agreement with the finding of Levaot et al. (Levaot et al., 2011b), mutant SH3BP2 protein levels were constitutively increased in TLR2- and TLR4-stimulated BMMs. To investigate a potential crosstalk between SYK and IKK activation in mutant BMMs, we compared phosphorylated IKKβ levels in BMMs stimulated with Pam3CSK4 or LPS in the presence or absence of BAY-613606. Increases of phosphorylation levels of IKKβ as well as IKKα at 240 minutes after stimulation were less in the presence of BAY-613606 (Figure 5C), suggesting that SYK activity is required for the increase in IKKβ activity in *Sh3bp2*$^{KI/KI}$ BMMs and that mutant SH3BP2 enhances NF-κB signaling by a mechanism that involves SYK.

SYK interacts with SH3BP2 in macrophages (Figure S3) and phosphorylates three tyrosine residues in SH3BP2 at Y174, Y183, and Y446 (Maeno et al., 2003). Phosphorylation of these tyrosines is critically involved in the immune response of T cells (Qu et al., 2005) and B cells (Shukla et al., 2009). Because overexpression of SH3BP2 in RAW264.7 cells phenocopies the increased TNF-α production in *Sh3bp2*$^{KI/KI}$ macrophages (Levaot et al., 2011b), we used these cells to examine to what extent these phosphorylated tyrosines are involved in TNF-α production. Wild-type and various tyrosine-mutated forms of SH3BP2 with or without the P416R cherubism mutation were overexpressed in RAW264.7 cells, and TNF-α levels in culture supernatants were measured. RAW264.7 cells overexpressing the Y174/183/446F (3F) and the Y183F form of SH3BP2 showed the most significant reduction in TNF-α production compared to overexpression of wild-type (3Y) SH3BP2 (Figure 5D), suggesting that Y183 phosphorylation is critical for SH3BP2 to induce TNF-α overproduction in a gain-of-function manner and that the amount of Y183-phosphorylated SH3BP2 correlates with enhanced TNF-α production.

Next, we examined whether the Y183 phosphorylation level is altered in *Sh3bp2*$^{KI/KI}$ BMMs stimulated with Pam3CSK4 or LPS. Western blotting analysis using an antibody that detects Y183-phosphorylated SH3BP2 (Figure S4) revealed that total Y183 phosphorylation is induced and increased in *Sh3bp2*$^{KI/KI}$ BMMs after 60 minutes compared to *Sh3bp2*$^{+/+}$ BMMs (Figure 5E). When SYK activity was inhibited, these phosphorylation levels were reduced (Figure 5F). Since phosphorylated Y183 creates a binding site for VAV (Shukla et al., 2009) that can activate NF-κB signaling (Costello et al., 1999; Hebeis et al., 2005), we

further investigated the phosphorylation levels of VAV. Y174 phosphorylation of VAV1 was increased in *Sh3bp2*$^{KI/KI}$ BMMs stimulated with Pam3CSK4 compared with *Sh3bp2*$^{+/+}$ BMMs (Figure 5G) and the elevated phosphorylation level was suppressed when SYK was inhibited (Figure 5H). Phosphorylation of SYK at Y346, which is increased in *Sh3bp2*$^{KI/KI}$ osteoclasts (Ueki et al., 2007) was at comparable levels in *Sh3bp2*$^{KI/KI}$ and *Sh3bp2*$^{+/+}$ BMMs (data not shown), suggesting that mutant SH3BP2 does not likely affect SYK activity during the time course observed and that increased Y183 phosphorylation in *Sh3bp2*$^{KI/KI}$ BMMs is due to increased protein levels of mutant SH3BP2. Collectively, these results suggest that increased levels of mutant SH3BP2 augment NF-κB pathway activation through SYK, and that Y183 phosphorylation in SH3BP2 by SYK leads to increased TNF-α production in *Sh3bp2*$^{KI/KI}$ macrophages.

Germ-free *Sh3bp2*$^{KI/KI}$ mice develop inflammation and bone loss

Sh3bp2$^{KI/KI}$ macrophage activation in response to PAMPs results in elevated TNF-α production (Figure 4A–H). Therefore, we speculated that depletion of the microbial flora in *Sh3bp2*$^{KI/KI}$ mice may ameliorate inflammation. To address this possibility, we created germ-free *Sh3bp2*$^{KI/KI}$ mice (axenic *Sh3bp2*$^{KI/KI}$ mice living in the absence of detectable microorganisms, Figure S5 for exclusion list) by rederiving and subsequent crossing of *Sh3bp2*$^{KI/+}$ mice in a sterile environment. Unexpectedly, germ-free *Sh3bp2*$^{KI/KI}$ mice developed substantial inflammation in face, lung, liver, stomach, and lymph nodes as well as calvarial bone loss (Figure 6A). Quantitative analysis revealed that the severity of liver inflammation (Figure 6B) and calvarial bone loss (Figure 6C) are even greater in germ-free *Sh3bp2*$^{KI/KI}$ mice than those in *Sh3bp2*$^{KI/KI}$ mice under specific-pathogen-free (SPF; Figure S5 for exclusion list) conditions. Serum TNF-α levels were decreased in germ-free *Sh3bp2*$^{KI/KI}$ mice compared to SPF *Sh3bp2*$^{KI/KI}$ mice (Figure 6D), but still elevated compared to SPF *Sh3bp2*$^{+/+}$ mice. These data suggest that bacterial components that stimulate TLR2 and TLR4 are not exclusive triggers of inflammation in cherubism mice.

Because inflammation in *Sh3bp2*$^{KI/KI}$ mice is primarily TLR2/4-dependent, this result further implies that TLR2 and TLR4 ligands derived from sources other than bacteria, such as DAMPs, are capable of inducing inflammation by activating MYD88-mediated signaling pathways. To test whether the cherubism mutation also sensitizes macrophage responses to DAMPs, *Sh3bp2*$^{KI/KI}$ BMMs were stimulated with serum amyloid A (SAA) or hyaluronic acid, which are DAMPs that can activate TLR2 and TLR4 (Piccinini and Midwood, 2010). In both cases, TNF-α levels were higher in *Sh3bp2*$^{KI/KI}$ BMM culture supernatants than in *Sh3bp2*$^{+/+}$ BMM supernatants (Figure 6E). *Sh3bp2*$^{KI/KI}$ BMM stimulation with biglycan exhibited similar results (data not shown). We further found that TNF-α-stimulated *Sh3bp2*$^{KI/KI}$ BMMs and liver tissues from *Sh3bp2*$^{KI/KI}$ mice (with no treatment) express increased amounts of SAA (Figure 6F, 6G). Cells that undergo programmed-necrosis (necroptosis) in response to TNF-α release DAMPs (Kaczmarek et al., 2013). This led us to examine the effect of necroptosis in the development of inflammation in *Sh3bp2*$^{KI/KI}$ mice. Administration of necrostatin-1 (Nec-1), an inhibitor of necroptosis (Christofferson and Yuan, 2010), to 1-week-old neonatal *Sh3bp2*$^{KI/KI}$ mice for 7 weeks significantly decreased liver inflammation (Figure 6H). However, serum TNF-α levels (Figure 6I) and inflammation in facial tissues, lung, and stomach (data not shown) were not substantially affected,

suggesting that DAMPs derived from necroptosis are only partially responsible for inflammation in *Sh3bp2*$^{KI/KI}$ mice in a tissue-specific manner.

SYK-dependent macrophage inflammation and bone loss in cherubism mice

Given the fact that SYK phosphorylates Y183 in SH3BP2 (Maeno et al., 2003) and this phosphorylation is important for TNF-α production in RAW264.7 cells (Figure 5D), we next questioned whether absence of SYK in macrophages may rescue cherubism mice from inflammation *in vivo*. To delete SYK in macrophages, we used *LysM-Cre* mice (Clausen et al., 1999) and generated cherubism mice in which SYK is selectively deficient in macrophages (*Sh3bp2*$^{KI/KI}$/*LysM-Cre*/*Syk*$^{fl/fl}$, hereafter referred to as *Sh3bp2*$^{KI/KI}$/*Syk*$^{\Delta M/\Delta M}$). The *Sh3bp2*$^{KI/KI}$/*Syk*$^{\Delta M/\Delta M}$ mice exhibited significantly reduced facial swelling, lung, liver, and stomach inflammation as well as calvarial bone loss (Figure 7A). Histomorphometric and microCT analysis confirmed the significant reduction of liver lesions (Figure 7B) and calvarial bone erosion (Figure 7C) in *Sh3bp2*$^{KI/KI}$/*Syk*$^{\Delta M/\Delta M}$ mice compared to *Sh3bp2*$^{KI/KI}$/*Syk*$^{fl/fl}$ mice. Consistent with these results, serum TNF-α was undetectable in *Sh3bp2*$^{KI/KI}$/*Syk*$^{\Delta M/\Delta M}$ mice (Figure 7D).

To examine whether SYK-deficient *Sh3bp2*$^{KI/KI}$ BMMs exhibit reduced TNF-α production in response to TLR2 and TLR4 activation, we cultured BMMs from *Sh3bp2*$^{KI/KI}$/*Mx1-Cre*/*Syk*$^{fl/fl}$ mice treated with Poly(I:C) (hereafter referred to as *Sh3bp2*$^{KI/KI}$/*Syk*$^{\Delta/\Delta}$), which allowed us to obtain bone marrow cells with nearly complete target gene deletion (Aliprantis et al., 2008). The *Sh3bp2*$^{KI/KI}$/*Syk*$^{\Delta/\Delta}$ BMMs produced reduced amounts of TNF-α compared to *Sh3bp2*$^{KI/KI}$/*Syk*$^{fl/fl}$ BMMs, which were comparable to control *Sh3bp2*$^{+/+}$/*Syk*$^{fl/fl}$ BMMs (Figure 7E). Western blotting analysis further revealed that phosphorylation levels of IKKα/β and IκB were reduced and that total IκB levels were increased in *Sh3bp2*$^{KI/KI}$/*Syk*$^{\Delta/\Delta}$ BMMs compared to *Sh3bp2*$^{KI/KI}$/*Syk*$^{fl/fl}$ BMMs (Figure 7F), suggesting that activation of the NF-κB pathway in *Sh3bp2*$^{KI/KI}$ BMMs stimulated with TLR2 and TLR4 ligands is reduced when SYK is deficient.

Overproduction of IL-1β is associated with a number of autoinflammatory diseases (Masters et al., 2009). Since IL-1R1-deficient *Sh3bp2*$^{KI/KI}$ mice showed a partial reduction in liver inflammation (Figure 3B), we hypothesized that mutant SH3BP2 may be involved in dysregulation of IL-1β production and that *Sh3bp2*$^{KI/KI}$ BMMs produce more IL-1β in response to TLR stimulation. Strikingly, IL-1β production in *Sh3bp2*$^{KI/KI}$ BMMs was increased compared to wild-type cells (Figure 7G), indicating that IL-1β is partially involved in the development or maintenance of inflammation in *Sh3bp2*$^{KI/KI}$ mice. This may explain the reduction in liver lesions in *Sh3bp2*$^{KI/KI}$/*Il1r1*$^{-/-}$mice (Figure 3B). We further examined whether mutant SH3BP2 enhances TNF-α-induced TNF-α expression in macrophages. Real-time PCR analysis revealed that TNF-α-stimulated *Sh3bp2*$^{KI/KI}$ BMMs express increased levels of TNF-α compared to *Sh3bp2*$^{+/+}$ and *Sh3bp2*$^{-/-}$BMMs (Figure 7H), suggesting an autoregulatory TNF-α inflammatory circuit that accelerates the development of cherubism lesions once inflammation has been initiated. Taken together, these data provide a basis for understanding the development of cherubism lesions in humans who are heterozygous for mutations in SH3BP2. After early induction of TNF-α production by M-CSF (Ueki et al., 2007) and following TLR ligand accumulation (this study), mutant

SH3BP2 gets involved in multiple inflammatory pathways in macrophages, leading to sustained and irreversible inflammation until puberty when the TLR-MYD88 pathway becomes less active, which results in the regression of cherubism lesions (Figure 7I).

Discussion

Jaw-specific development of cherubism lesions

Significant rescue of inflammation in TLR2/TLR4-deficient *Sh3bp2*$^{KI/KI}$ mice and increased responses to TLR ligands in *Sh3bp2*$^{KI/KI}$ BMMs suggest that TLR2 and TLR4 stimulation play a major role in the development of inflammation in cherubism mice. TLR2 and TLR4 are primary receptors for microbial pathogens (Akira et al., 2006) and microorganisms play important roles in the induction and progression of immune diseases by modulating crosstalk between the innate and adaptive immune systems (Chervonsky, 2010). Jaws are located in proximity to the oral cavity which harbors a variety of commensal and pathogenic microorganisms that provide ligands for TLR2 and TLR4 (Mogensen, 2009; Wade, 2013). The large number of pathogenic bacteria in the oral cavity includes *Porphyromonas gingivalis* that activates TLR2 and is responsible for the common oral disease periodontitis (Burns et al., 2006; Darveau, 2010). Dental plaques containing various other microorganisms can also activate either TLR2 or TLR4 responses (Yoshioka et al., 2008). Therefore, it is possible that a change in microbial load in the oral cavity in early childhood may contribute to the jaw-specificity in cherubism patients. As a result, it is conceivable that intensive oral health care or antibiotics treatment to reduce pathogenic oral microorganisms may ameliorate or delay cherubism symptoms.

However, the fact that germ-free cherubism mice still develop inflammation (Figure 6A–D) indicates that DAMPs that stimulate TLR2- and TLR4-mediated local immune system could also be involved in the development of human cherubism lesions. Indeed, a variety of DAMPs can serve as ligands for TLR2 and/or TLR4 (Chen and Nunez, 2010; Piccinini and Midwood, 2010; Zhang and Mosser, 2008). Jaws are exposed to unique challenges since they are subject to increased tissue and bone remodeling due to tooth eruption and strain caused by mastication. A large amount of DAMPs may be generated in human jaw tissues during tooth eruption and the associated damage to gingival tissues. DAMPs may also be generated as a result of bone remodeling associated with repair of microfractures caused by the mechanical stress of mastication. Huja et al. reported that bone turnover in the maxilla and mandible of dogs is higher than in the femoral bone, and that bone formation rate in the dog jaw remains high during skeletal maturation, while it decreases with age in femurs (Huja and Beck, 2008; Huja et al., 2006). In addition, mechanical stimulation promotes the secretion of type I collagen and matrix degrading enzymes from human periodontal fibroblasts (Kook et al., 2011; Lisboa et al., 2013), suggesting that mastication contributes to DAMPs production. Taken together, these findings support the idea that jaw tissues are great sources of DAMPs for stimulating the local immune system through TLRs. In fact, development of active cherubism lesions in humans usually begins at 2–5 years of age (Reichenberger et al., 2012), which coincides with the development of the secondary dentition accompanied by increased jawbone remodeling. Therefore, it is possible that abundant generation of DAMPs in jaw tissues contributes to the jaw-specific development

of cherubism lesions. Consequently, we hypothesize that stimulation of TLRs as a result of abundant production of both PAMPs and DAMPs in the jaws may be the major cause of jaw-specific development of human cherubism lesions. Examination of inflammatory cytokine production in macrophages of cherubism patients in response to TLR ligands would be required to confirm our hypothesis.

Age-dependent regression of cherubism lesions

Jaw growth and remodeling stabilize with age due to completion of primary tooth loss and eruption of permanent teeth, suggesting that production of DAMPs in the jaw that stimulate TLRs decreases after puberty. Therefore, we speculate that regression of cherubism lesions in humans can, at least in part, be attributed to the decreased release of DAMPs in the jaw. On the other hand, the innate immune system in humans is affected by age (Kollmann et al., 2012; Shaw et al., 2013). Therefore, a mechanism that regulates age-dependent innate immune response may contribute to the age-dependent regression. We demonstrated here that increased activation of the MYD88-mediated pathway in macrophages plays a key role in the inflammation in *Sh3bp2*$^{KI/KI}$ mice. In contrast, loss of function mutations in MYD88 and IL-1R-associated kinase 4 (IRAK4), a protein that interacts with MYD88 and cooperatively activates downstream NF-κB signaling, cause a condition of primary immunodeficiency (PID) in humans that is particularly susceptible to infection by pyogenic bacteria. Interestingly, the clinical condition of MYD88- and IRAK4-deficient patients improves with age (Ku et al., 2007; von Bernuth et al., 2008). The observation that both MYD88- and IRAK4-deficient patients are affected mostly in the neonatal and childhood period and appear to show clinical improvement in adolescence suggests age-dependent maturation of TLR-independent innate immunity or establishment of antigen-specific adaptive immunity by T and B lymphocytes to the morbid bacteria (Mogensen, 2009; Picard et al., 2010; von Bernuth et al., 2008). Because two different MYD88-associated disorders, PID and cherubism, show similar dramatic improvement of symptoms with age, MYD88-dependent immunity seems to become redundant and less important later in life (Casanova et al., 2011; von Bernuth et al., 2008). Therefore, we suggest that reduced involvement of the MYD88-mediated pathway in macrophage activation could be another potential reason for the regression of cherubism lesions after puberty. In addition, a decline of growth hormone after sexual and physical maturation might modulate the process of age-dependent regression (Masternak and Bartke, 2012).

Comparison of cherubism mouse model to human cherubism

The *Sh3bp2* cherubism mouse model replicates many features of cherubism (Ueki et al., 2007). However, mode of the inheritance is different between human and mouse, and most studies in the cherubism mouse model have been conducted in homozygous *Sh3bp2*$^{KI/KI}$ mice where the phenotype is strongly expressed. Evolutionary changes in the precise roles of human and mouse orthologs often cause equivalent mutations to have different phenotypic effects in the two species (Liao and Zhang, 2008). SH3BP2 function may be more critical in humans than in mice and it may take longer for heterozygous cherubism mice to develop any inflammatory phenotype. On the other hand, our results showed that TNF-α production levels in heterozygous *Sh3bp2*$^{KI/+}$ BMMs in response to PAMPs and DAMPs are also elevated compared to *Sh3bp2*$^{+/+}$ BMMs (Figure 4, 6E). Therefore, the

absence of inflammatory lesions in heterozygous *Sh3bp2*$^{KI/+}$ mice may be due to insufficient generation of TLR ligands under animal facility conditions. Forced chronic stimulation of *Sh3bp2*$^{KI/+}$ mice with TLR ligands or maintaining them in a contaminated environment for extended periods of time may induce the development of inflammatory lesions in *Sh3bp2*$^{KI/+}$ mice.

TLR ligands that trigger inflammation in cherubism mice

Since overall inflammation in germ-free *Sh3bp2*$^{KI/KI}$ mice is comparable to that in SPF *Sh3bp2*$^{KI/KI}$ mice, the effect of PAMPs on the development of inflammation in our SPF facility is likely to be limited. Therefore, we conclude that DAMPs, including SAA produced by activated *Sh3bp2*$^{KI/KI}$ BMMs and liver tissues or hyaluronic acid (Figure 6E–G), are potential strong inducers of inflammation in *Sh3bp2*$^{KI/KI}$ mice. Another potential DAMP for the development of inflammation in *Sh3bp2*$^{KI/KI}$ mice is biglycan. Biglycan-dependent cytokine production by macrophages is completely abolished in *Tlr2*$^{-/-}$/*Tlr4*$^{-/-}$mice, and biglycan-null mice are resistant to LPS- or zymosan-induced sepsis due to reduced TNF-α production (Schaefer et al., 2005). These findings suggest that extracellular matrix molecules can contribute to the induction of inflammation by binding to TLR2 and TLR4. The actual *in vivo* TLR2 and TLR4 ligands and their relative contributions to the inflammation in *Sh3bp2*$^{KI/KI}$ mice have not been determined in this study, but TLR2 seemed to be involved to a greater extent than TLR4 in reduction of serum TNF-α levels and liver lesions (Figure S6). Investigation of DAMPs that can provoke inflammatory responses in cherubism mice will provide new therapeutic targets not only for cherubism but also for other autoinflammatory diseases (Park et al., 2012) and sterile inflammation (Chen and Nunez, 2010). However, because *Sh3bp2*$^{KI/KI}$/*Tlr2*$^{-/-}$/*Tlr4*$^{lps\text{-}del/lps\text{-}del}$ mice still exhibit a detectable phenotype compared to *Sh3bp2*$^{KI/KI}$/*Myd88*$^{-/-}$mice, we cannot exclude the possibility that ligands for TLRs other than TLR2 and TLR4 or non-TLRs that use MYD88 (Adachi et al., 1998; Sun and Ding, 2006) contribute to the inflammation in *Sh3bp2*$^{KI/KI}$ mice.

Mutant SH3BP2 enhances macrophage activation through SYK

The effect of SYK deficiency on the reduction of TNF-α production is more significant in *Sh3bp2*$^{KI/KI}$ BMMs than in *Sh3bp2*$^{+/+}$ BMMs (Figure 7E). This suggests that involvement of SYK in TNF-α production is greater in *Sh3bp2*$^{KI/KI}$ BMMs than in *Sh3bp2*$^{+/+}$ BMMs and that SYK is largely involved in the signaling pathway that enhances NF-κB pathway in cooperation with mutant SH3BP2.

Our study demonstrates that Y183 phosphorylation in SH3BP2 is essential for the gain of SH3BP2 function that leads to TNF-α overproduction in macrophages (Figure 5D). The overall increased Y183 phosphorylation levels in *Sh3bp2*$^{KI/KI}$ BMMs after TLR stimulation compared to *Sh3bp2*$^{+/+}$ BMMs (Figure 5E) is consistent with this result. However, the degree to which the Y183 residue of SH3BP2 is phosphorylated was not increased in RAW264.7 cells overexpressing the P416R SH3BP2 (Figure S7), suggesting that the P416R mutation does not accelerate the Y183 phosphorylation. Therefore, increased levels of total Y183 phosphorylation in *Sh3bp2*$^{KI/KI}$ BMM can be attributed to the elevated amounts of total SH3BP2 protein, even though the ratio to total SH3BP2 protein is decreased. Since

SYK phosphorylates the Y183 residue in SH3BP2 (Maeno et al., 2003), reduction of Y183 phosphorylation by a SYK inhibitor could be a potential therapeutic option for the cherubism treatment. Indeed, SYK ablation in macrophages rescues *Sh3bp2*$^{KI/KI}$ mice from inflammation.

Our study provides novel insights into a mechanism of macrophage activation and autoinflammation via SH3BP2. We demonstrated the important role of mutant SH3BP2 in activation of the TLR-MYD88-NF-κB signaling axis in macrophages, resulting in TNF-α-driven autoinflammation and the function of SH3BP2 as an adaptor that links SYK to NF-κB activation. Although symptoms and disease processes in *Sh3bp2*$^{KI/KI}$ mice are not completely identical to cherubism in humans, we believe that the cherubism mice and human cherubism patients share common pathogenetic mechanisms. The involvement of the TLR-MYD88 signaling pathway provides a novel framework for addressing the unresolved questions of why cherubism lesions in humans are primarily localized to the jaws and why they exhibit age-dependent regression after puberty. Therapeutically, our results suggest that SYK inhibitors may be effective in the treatment of cherubism.

Experimental Procedures

Mice

Sh3bp2$^{KI/KI}$ mice were reported previously (Ueki et al., 2007). *Sh3bp2*$^{-/-}$mutant (Chen et al., 2007) is a gift from Dr. Rottapel. *Myd88*$^{-/-}$mice (Adachi et al., 1998) were provided by Dr. Akira. *Tlr2*$^{-/-}$(004650), *Tlr4*$^{lps\text{-}del/lps\text{-}del}$ (007227), *Il1r1*$^{-/-}$(003245), *Mx1-Cre* (003556), *LysM-Cre* (004781), and *Syk*$^{fl/fl}$ (017309) mice were obtained from the Jackson Laboratory (Bar Harbor, ME). All strains are on C57BL/6 background and housed in a specific-pathogen-free (SPF) environment at University of Missouri-Kansas City. Germ-free *Sh3bp2*$^{KI/KI}$ mice were created by Taconic (Hudson, NY) after rederivation of SPF-*Sh3bp2*$^{KI/+}$ mice and subsequent crossing with germ-free *Sh3bp2*$^{KI/+}$ mice. Germ-free shipper was used for delivery (Figure S5). Tissue and serum of germ-free mice were harvested immediately after arrival. To obtain SYK-deficient bone marrow cells, 4–6-week old *Syk*$^{fl/fl}$/*Mx1-Cre* mice were injected with Poly(I:C) (250 μg/body, GE Healthcare, Pittsburgh, PA) intraperitoneally 3 times with 2-day intervals. All experiments were performed in accordance with the guidelines of the Institutional Animal Care and Use Committee of the University of Missouri-Kansas City.

Tissue preparation and histomorphometric analysis of liver inflammation

Tissues were fixed in 4% paraformaldehyde/PBS or Bouin's solution and embedded in paraffin. Sections (6 μm) were stained with hematoxylin and eosin (H&E). To assess the inflammation in liver tissues, total inflammatory area in a liver image was measured as pixels with ImageJ (NIH), and divided by the pixels of the entire tissue image to calculate the proportion of inflammatory area (%). Areas of vasculature were excluded from entire tissue area. The formula used is: Inflammatory area (%) = 100 × (total inflamed area) / {(total tissue area) – (total vascular area)}. Liver images were taken with 4X objective lens (E800, NIKON Instruments Inc., Melville, NY). Results from three to five images from different areas of each tissue section were averaged.

Micro-computed tomography (microCT) analysis

Paraformaldehyde-fixed calvarial tissues were subjected to microCT (vivaCT 40, Scanco Medical, Wayne, PA) analysis. Resulting images were used to quantitate inflammatory bone erosion in calvarial bone. Two-dimensional images were taken with a threshold of 300 for mineralized tissue and further processed for the three-dimensional (3D) image reconstruction with a spatial resolution of 10 μm. 3D images (6 mm × 6 mm) were used to calculate the proportion of erosion area (%) of calvarial bone. The intersection of the coronal and sagittal sutures was used as a reference position of the square center. Total area of bone erosion including suture area in 6 mm × 6 mm calvarial bone images was measured as pixels with ImageJ and divided by the total number of pixels.

Bone marrow-derived M-CSF-dependent macrophage (BMM) cultures

Bone marrow cells were harvested from femur, tibia, and pelvic bones of 6 to 12-week-old mice. After red blood cell lysis, cells were pre-incubated with α-MEM supplemented with 10% fetal bovine serum (FBS) for 2–12 hours on Petri dishes. Non-adherent cells were collected and cultured for 4–5 days with α-MEM supplemented with 10% FBS, penicillin/streptomycin, and 30 ng/ml of murine M-CSF (Peprotech, Rocky Hill, NJ) on Petri dishes. Adherent BMMs were harvested and 4.8×10^4 cells/well were plated in 96-well plates without M-CSF for ELISA.

Statistical analysis

Mean value comparison between two groups was performed with Student's t-test (two-tailed distribution, equal variance). One-way ANOVA was used to compare means among three or more groups. If the ANOVA showed a significant difference, Tukey-Kramer test was used as a post-hoc test. $p < 0.05$ was considered as statistically significant.

Supplementary Material

Refer to Web version on PubMed Central for supplementary material.

Acknowledgments

We thank members of Bone Biology Research Program at the University of Missouri-Kansas City for critical suggestions. We also thank Drs. Rottapel and Akira for providing SH3BP2- and MYD88-deficient mice respectively. This work was supported by a grant from the NIH (R01DE020835) to YU. TM is a recipient of 2009 Japan Rheumatism Foundation Traveling Fellowship and 2011 ASBMR Young Investigator Award.

References

Adachi O, Kawai T, Takeda K, Matsumoto M, Tsutsui H, Sakagami M, Nakanishi K, Akira S. Targeted disruption of the MyD88 gene results in loss of IL-1- and IL-18-mediated function. Immunity. 1998; 9:143–150. [PubMed: 9697844]

Akira S, Uematsu S, Takeuchi O. Pathogen recognition and innate immunity. Cell. 2006; 124:783–801. [PubMed: 16497588]

Aliprantis AO, Ueki Y, Sulyanto R, Park A, Sigrist KS, Sharma SM, Ostrowski MC, Olsen BR, Glimcher LH. NFATc1 in mice represses osteoprotegerin during osteoclastogenesis and dissociates systemic osteopenia from inflammation in cherubism. J Clin Invest. 2008; 118:3775–3789. [PubMed: 18846253]

Berendsen AD, Olsen BR. Tankyrase loses its grip on SH3BP2 in cherubism. Cell. 2011; 147:1222–1223. [PubMed: 22153068]

Burns E, Bachrach G, Shapira L, Nussbaum G. Cutting Edge: TLR2 is required for the innate response to Porphyromonas gingivalis: activation leads to bacterial persistence and TLR2 deficiency attenuates induced alveolar bone resorption. J Immunol. 2006; 177:8296–8300. [PubMed: 17142724]

Casanova JL, Abel L, Quintana-Murci L. Human TLRs and IL-1Rs in host defense: natural insights from evolutionary, epidemiological, and clinical genetics. Annu Rev Immunol. 2011; 29:447–491. [PubMed: 21219179]

Chen G, Dimitriou ID, La Rose J, Ilangumaran S, Yeh WC, Doody G, Turner M, Gommerman J, Rottapel R. The 3BP2 adapter protein is required for optimal B-cell activation and thymus-independent type 2 humoral response. Mol Cell Biol. 2007; 27:3109–3122. [PubMed: 17283041]

Chen GY, Nunez G. Sterile inflammation: sensing and reacting to damage. Nat Rev Immunol. 2010; 10:826–837. [PubMed: 21088683]

Chervonsky AV. Influence of microbial environment on autoimmunity. Nat Immunol. 2010; 11:28–35. [PubMed: 20016507]

Christofferson DE, Yuan J. Necroptosis as an alternative form of programmed cell death. Curr Opin Cell Biol. 2010; 22:263–268. [PubMed: 20045303]

Clausen BE, Burkhardt C, Reith W, Renkawitz R, Forster I. Conditional gene targeting in macrophages and granulocytes using LysMcre mice. Transgenic research. 1999; 8:265–277. [PubMed: 10621974]

Costello PS, Walters AE, Mee PJ, Turner M, Reynolds LF, Prisco A, Sarner N, Zamoyska R, Tybulewicz VL. The Rho-family GTP exchange factor Vav is a critical transducer of T cell receptor signals to the calcium, ERK, and NF-kappaB pathways. Proc Natl Acad Sci U S A. 1999; 96:3035–3040. [PubMed: 10077632]

Darveau RP. Periodontitis: a polymicrobial disruption of host homeostasis. Nature reviews Microbiology. 2010; 8:481–490.

Deckert M, Tartare-Deckert S, Hernandez J, Rottapel R, Altman A. Adaptor function for the Syk kinases-interacting protein 3BP2 in IL-2 gene activation. Immunity. 1998; 9:595–605. [PubMed: 9846481]

Ferguson PJ, El-Shanti HI. Autoinflammatory bone disorders. Curr Opin Rheumatol. 2007; 19:492–498. [PubMed: 17762617]

Foucault I, Le Bras S, Charvet C, Moon C, Altman A, Deckert M. The adaptor protein 3BP2 associates with VAV guanine nucleotide exchange factors to regulate NFAT activation by the B-cell antigen receptor. Blood. 2005; 105:1106–1113. [PubMed: 15345594]

Guettler S, LaRose J, Petsalaki E, Gish G, Scotter A, Pawson T, Rottapel R, Sicheri F. Structural basis and sequence rules for substrate recognition by Tankyrase explain the basis for cherubism disease. Cell. 2011; 147:1340–1354. [PubMed: 22153077]

Hebeis B, Vigorito E, Kovesdi D, Turner M. Vav proteins are required for B-lymphocyte responses to LPS. Blood. 2005; 106:635–640. [PubMed: 15811961]

Huja SS, Beck FM. Bone remodeling in maxilla, mandible, and femur of young dogs. Anat Rec (Hoboken). 2008; 291:1–5. [PubMed: 18085627]

Huja SS, Fernandez SA, Hill KJ, Li Y. Remodeling dynamics in the alveolar process in skeletally mature dogs. Anat Rec A Discov Mol Cell Evol Biol. 2006; 288:1243–1249. [PubMed: 17075846]

Jevremovic D, Billadeau DD, Schoon RA, Dick CJ, Leibson PJ. Regulation of NK cell-mediated cytotoxicity by the adaptor protein 3BP2. J Immunol. 2001; 166:7219–7228. [PubMed: 11390470]

Kaczmarek A, Vandenabeele P, Krysko DV. Necroptosis: the release of damage-associated molecular patterns and its physiological relevance. Immunity. 2013; 38:209–223. [PubMed: 23438821]

Kawai T, Akira S. The role of pattern-recognition receptors in innate immunity: update on Toll-like receptors. Nat Immunol. 2010; 11:373–384. [PubMed: 20404851]

Kollmann TR, Levy O, Montgomery RR, Goriely S. Innate immune function by Toll-like receptors: distinct responses in newborns and the elderly. Immunity. 2012; 37:771–783. [PubMed: 23159225]

Kono H, Rock KL. How dying cells alert the immune system to danger. Nat Rev Immunol. 2008; 8:279–289. [PubMed: 18340345]

Kook SH, Jang YS, Lee JC. Involvement of JNK-AP-1 and ERK-NF-kappaB signaling in tension-stimulated expression of type I collagen and MMP-1 in human periodontal ligament fibroblasts. J Appl Physiol (1985). 2011; 111:1575–1583. [PubMed: 21757573]

Ku CL, von Bernuth H, Picard C, Zhang SY, Chang HH, Yang K, Chrabieh M, Issekutz AC, Cunningham CK, Gallin J, et al. Selective predisposition to bacterial infections in IRAK-4-deficient children: IRAK-4-dependent TLRs are otherwise redundant in protective immunity. J Exp Med. 2007; 204:2407–2422. [PubMed: 17893200]

Levaot N, Simoncic PD, Dimitriou ID, Scotter A, La Rose J, Ng AH, Willett TL, Wang CJ, Janmohamed S, Grynpas M, et al. 3BP2-deficient mice are osteoporotic with impaired osteoblast and osteoclast functions. J Clin Invest. 2011a; 121:3244–3257. [PubMed: 21765218]

Levaot N, Voytyuk O, Dimitriou I, Sircoulomb F, Chandrakumar A, Deckert M, Krzyzanowski PM, Scotter A, Gu S, Janmohamed S, et al. Loss of Tankyrase-Mediated Destruction of 3BP2 Is the Underlying Pathogenic Mechanism of Cherubism. Cell. 2011b; 147:1324–1339. [PubMed: 22153076]

Liao BY, Zhang J. Null mutations in human and mouse orthologs frequently result in different phenotypes. Proc Natl Acad Sci U S A. 2008; 105:6987–6992. [PubMed: 18458337]

Lisboa RA, Andrade MV, Cunha-Melo JR. Toll-like receptor activation and mechanical force stimulation promote the secretion of matrix metalloproteinases 1, 3 and 10 of human periodontal fibroblasts via p38, JNK and NF-kB. Arch Oral Biol. 2013; 58:731–739. [PubMed: 23332208]

Maeno K, Sada K, Kyo S, Miah SM, Kawauchi-Kamata K, Qu X, Shi Y, Yamamura H. Adaptor protein 3BP2 is a potential ligand of Src homology 2 and 3 domains of Lyn protein-tyrosine kinase. J Biol Chem. 2003; 278:24912–24920. [PubMed: 12709437]

Masternak MM, Bartke A. Growth hormone, inflammation and aging. Pathobiology of aging & age related diseases. 2012; 2

Masters SL, Simon A, Aksentijevich I, Kastner DL. Horror autoinflammaticus: the molecular pathophysiology of autoinflammatory disease (*). Annu Rev Immunol. 2009; 27:621–668. [PubMed: 19302049]

Mogensen TH. Pathogen recognition and inflammatory signaling in innate immune defenses. Clin Microbiol Rev. 2009; 22:240–273. [PubMed: 19366914]

O'Neill LA, Bowie AG. The family of five: TIR-domain-containing adaptors in Toll-like receptor signalling. Nat Rev Immunol. 2007; 7:353–364. [PubMed: 17457343]

Park H, Bourla AB, Kastner DL, Colbert RA, Siegel RM. Lighting the fires within: the cell biology of autoinflammatory diseases. Nat Rev Immunol. 2012; 12:570–580. [PubMed: 22828911]

Picard C, von Bernuth H, Ghandil P, Chrabieh M, Levy O, Arkwright PD, McDonald D, Geha RS, Takada H, Krause JC, et al. Clinical features and outcome of patients with IRAK-4 and MyD88 deficiency. Medicine (Baltimore). 2010; 89:403–425. [PubMed: 21057262]

Piccinini AM, Midwood KS. DAMPening inflammation by modulating TLR signalling. Mediators Inflamm. 2010

Qu X, Kawauchi-Kamata K, Miah SM, Hatani T, Yamamura H, Sada K. Tyrosine phosphorylation of adaptor protein 3BP2 induces T cell receptor-mediated activation of transcription factor. Biochemistry. 2005; 44:3891–3898. [PubMed: 15751964]

Reichenberger EJ, Levine MA, Olsen BR, Papadaki ME, Lietman SA. The role of SH3BP2 in the pathophysiology of cherubism. Orphanet J Rare Dis. 2012; 7(Suppl 1):S5. [PubMed: 22640988]

Ren R, Mayer BJ, Cicchetti P, Baltimore D. Identification of a ten-amino acid proline-rich SH3 binding site. Science. 1993; 259:1157–1161. [PubMed: 8438166]

Schaefer L, Babelova A, Kiss E, Hausser HJ, Baliova M, Krzyzankova M, Marsche G, Young MF, Mihalik D, Gotte M, et al. The matrix component biglycan is proinflammatory and signals through Toll-like receptors 4 and 2 in macrophages. J Clin Invest. 2005; 115:2223–2233. [PubMed: 16025156]

Shaw AC, Goldstein DR, Montgomery RR. Age-dependent dysregulation of innate immunity. Nat Rev Immunol. 2013; 13:875–887. [PubMed: 24157572]

Shukla U, Hatani T, Nakashima K, Ogi K, Sada K. Tyrosine phosphorylation of 3BP2 regulates B cell receptor-mediated activation of NFAT. J Biol Chem. 2009; 284:33719–33728. [PubMed: 19833725]

Sun D, Ding A. MyD88-mediated stabilization of interferon-gamma-induced cytokine and chemokine mRNA. Nat Immunol. 2006; 7:375–381. [PubMed: 16491077]

Takeuchi O, Hoshino K, Kawai T, Sanjo H, Takada H, Ogawa T, Takeda K, Akira S. Differential roles of TLR2 and TLR4 in recognition of gram-negative and gram-positive bacterial cell wall components. Immunity. 1999; 11:443–451. [PubMed: 10549626]

Ueki Y, Lin CY, Senoo M, Ebihara T, Agata N, Onji M, Saheki Y, Kawai T, Mukherjee PM, Reichenberger E, et al. Increased myeloid cell responses to M-CSF and RANKL cause bone loss and inflammation in SH3BP2 “cherubism” mice. Cell. 2007; 128:71–83. [PubMed: 17218256]

Ueki Y, Tiziani V, Santanna C, Fukai N, Maulik C, Garfinkle J, Ninomiya C, doAmaral C, Peters H, Habal M, et al. Mutations in the gene encoding c-Abl-binding protein SH3BP2 cause cherubism. Nat Genet. 2001; 28:125–126. [PubMed: 11381256]

von Bernuth H, Picard C, Jin Z, Pankla R, Xiao H, Ku CL, Chrabieh M, Mustapha IB, Ghandil P, Camcioglu Y, et al. Pyogenic bacterial infections in humans with MyD88 deficiency. Science. 2008; 321:691–696. [PubMed: 18669862]

Wade WG. The oral microbiome in health and disease. Pharmacol Res. 2013; 69:137–143. [PubMed: 23201354]

Yoshioka H, Yoshimura A, Kaneko T, Golenbock DT, Hara Y. Analysis of the activity to induce toll-like receptor (TLR)2- and TLR4-mediated stimulation of supragingival plaque. J Periodontol. 2008; 79:920–928. [PubMed: 18454672]

Yoshitaka T, Ishida S, Mukai T, Kittaka M, Reichenberger EJ, Ueki Y. Etanercept Administration to Neonatal SH3BP2 Knock-In Cherubism Mice Prevents TNF-α-induced Inflammation and Bone Loss. J Bone Miner Res. 2014; 29:1170–1182. [PubMed: 24978678]

Zhang X, Mosser DM. Macrophage activation by endogenous danger signals. J Pathol. 2008; 214:161–178. [PubMed: 18161744]

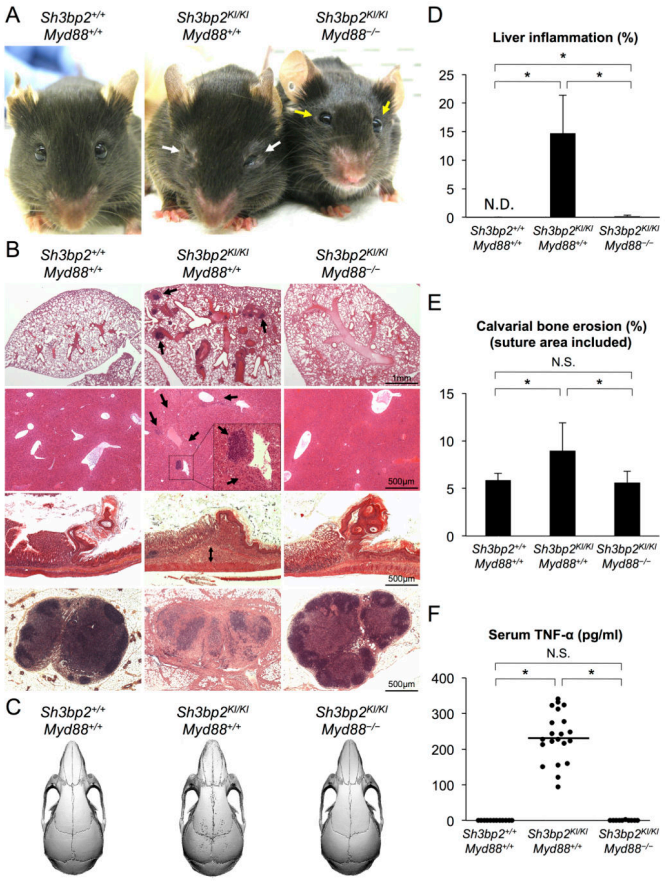

Figure 1. Lack of MYD88 rescues *Sh3bp2*$^{KI/KI}$ mice from inflammation

(A) Facial appearance of 10-week-old mice. Note the open eyelids, which represent lack of facial inflammation in double mutant mouse (*Sh3bp2*$^{KI/KI}$/*Myd88*$^{-/-}$, yellow arrows) compared to the inflamed control mouse (*Sh3bp2*$^{KI/KI}$/*Myd88*$^{+/+}$, white arrows). (B) H&E staining of tissues from 10-week-old mice (from top: lung, liver, stomach, and lymph node). Arrows indicate the inflammatory lesions in lung and liver. Double-headed arrow in stomach indicates the submucosal inflammatory cell infiltration rich in macrophages. (C) MicroCT image of the calvarial bone from 10-week-old mice. (D) Histomorphometric analysis of liver lesions in 10-week-old mice. n = 8–16 (E) Quantitative measurement of calvarial bone erosion in 10-week-old mice. n = 7–11 (F) Serum TNF-α levels in 10-week-old mice. n = 10–21. Horizontal bar represents average. Error bars represent ± SD. *p < 0.05. N.D.= not detected. N.S.= not significant. See also Figure S1.

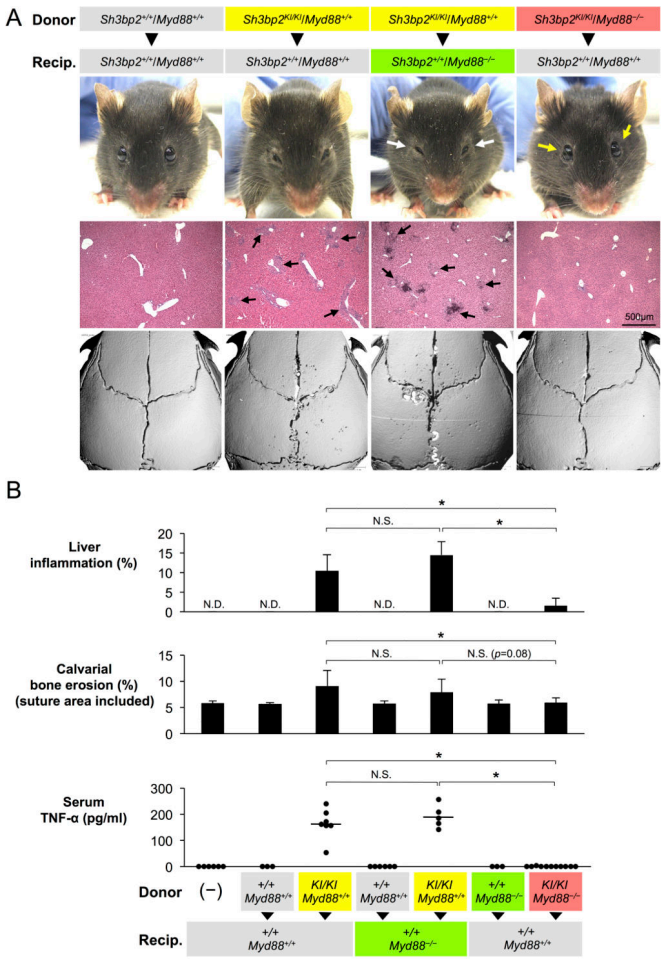

Figure 2. MYD88-mediated pathway in hematopoietic cells is responsible for inflammation in *Sh3bp2*$^{KI/KI}$ mice

(A) Facial appearance (top), H&E staining of liver tissue (middle), and calvarial bone microCT image (bottom) of bone marrow chimeric mice (13 weeks after transplantation). Busulfan-treated 4 to 5-week-old recipient mice (recip.) were transplanted with bone marrow (BM) cells from 4-week-old donor mice. Note the open eyes (yellow arrows), and reduced liver inflammation and calvarial bone erosion in *Sh3bp2*$^{+/+}$/*Myd88*$^{+/+}$ mouse transplanted with *Sh3bp2*$^{KI/KI}$/*Myd88*$^{-/-}$BM cells compared to *Sh3bp2*$^{+/+}$/*Myd88*$^{-/-}$mouse transplanted with *Sh3bp2*$^{KI/KI}$/*Myd88*$^{+/+}$ BM cells. White and black arrows indicate closed eyelids due to facial skin inflammation and severe liver lesions, respectively. (B) Histomorphometric analysis of liver lesions (n = 3–11), quantitative measurement of calvarial bone erosion (n = 3–7), and serum TNF-α levels (*n* = 3–11) of recipient mice 13 weeks after transplantation. Horizontal bars represent average. Error bars represent ± SD. *p < 0.05. N.D.= not detected. N.S.= not significant.

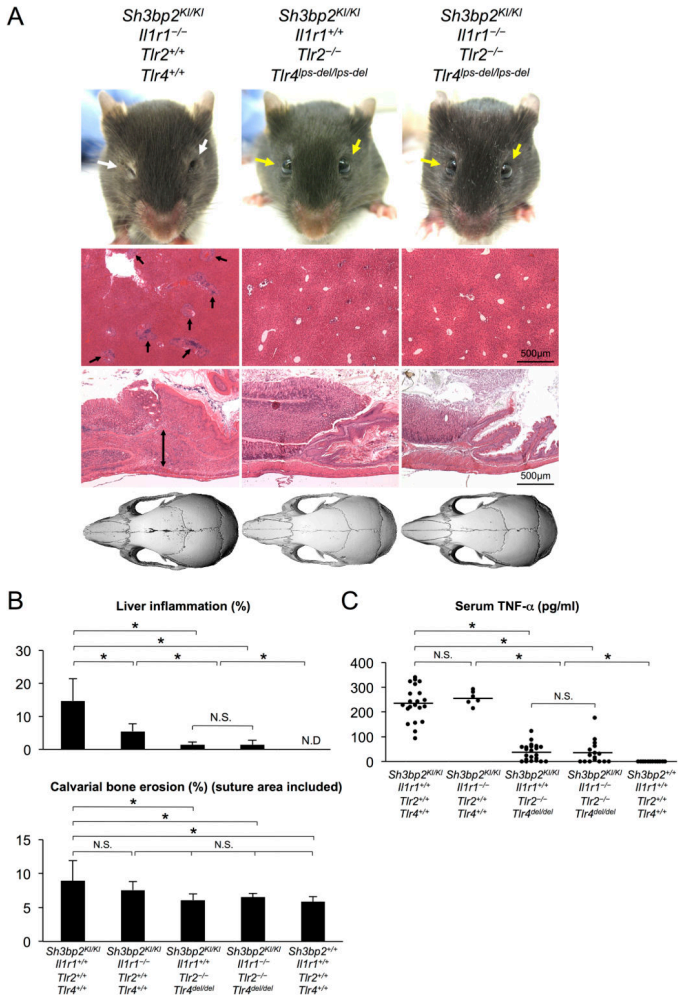

Figure 3. Absence of TLR2 and TLR4 rescues inflammation in *Sh3bp2*$^{KI/KI}$ mice

(A) Facial appearance (top), H&E staining of liver and stomach tissues (middle), and calvarial bone microCT image (bottom) of IL-1R1-deficient *Sh3bp2*$^{KI/KI}$, TLR2/TLR4-deficient *Sh3bp2*$^{KI/KI}$, and IL-1R1/TLR2/TLR4-deficient *Sh3bp2*$^{KI/KI}$ mice at 10 weeks of age. Yellow arrows indicate open eyelids representing rescued facial inflammation. White arrows indicate closed eyelids due to un-rescued facial inflammation. Black arrows indicate inflammatory lesions in liver and stomach. (B) Histomorphometric analysis of liver lesions (n = 7–17) and quantitative measurement of calvarial bone erosion (n = 7–11) in 10-week-old mice. (C) TNF-α levels in serum of 10-week-old mice. n = 6–22. Horizontal bars represent average. Error bars represent ± SD. *p < 0.05. N.D.= not detected. N.S.= not significant. *Tlr4*$^{del/del}$ = *Tlr4*$^{lps\text{-}del/lps\text{-}del}$.

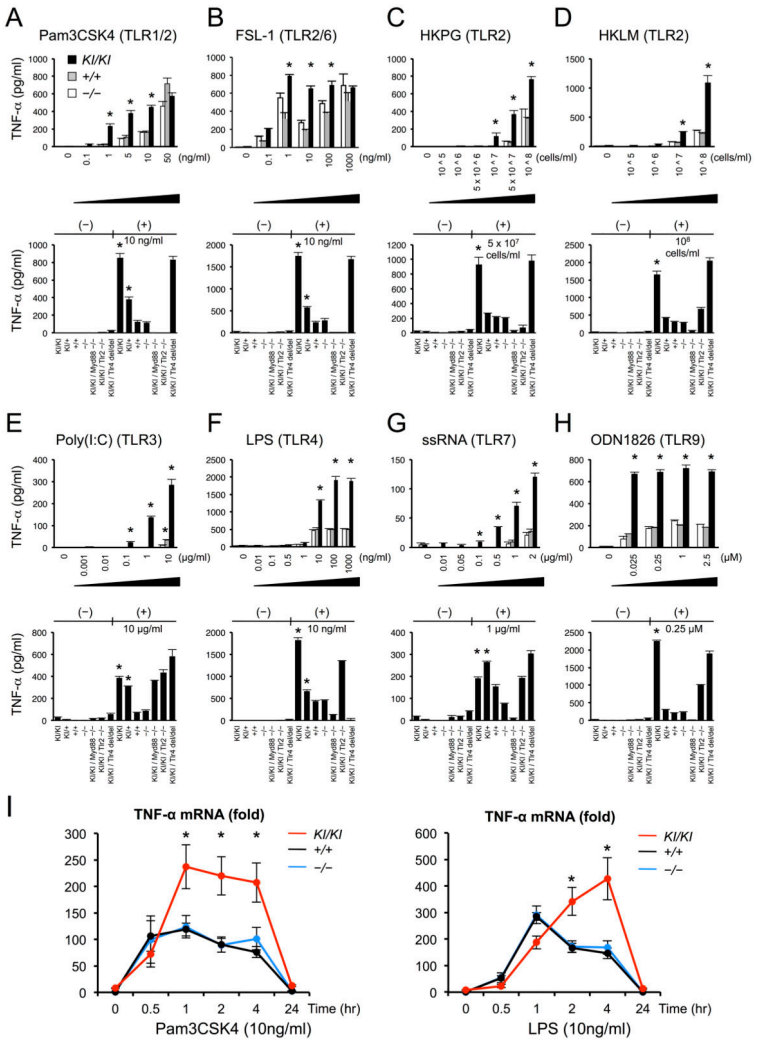

Figure 4. Increased response to TLR ligands in *Sh3bp2*$^{KI/KI}$ macrophages

(A–H) TNF-α levels in culture supernatants of BMMs stimulated with TLR ligands. BMMs from *Sh3bp2*$^{KI/KI}$ (*KI/KI*), *Sh3bp2*$^{+/+}$ (+/+), and *Sh3bp2*$^{-/-}$(−/−) mice were cultured in the absence of M-CSF for 4 to 6 hours, then stimulated for 24 hours with (A) Pam3CSK4, (B) FSL-1, (C) heat killed *Porphyromonas gingivalis* (HKPG), (D) heat killed *Listeria monocytogenes*, (E) Poly(I:C), (F) LPS, (G) ssRNA, and (H) CpG oligo DNA. Dose-dependent effects of TLR stimulation on TNF-α production (upper) and the critical role of MYD88 in TNF-α production in *Sh3bp2*$^{KI/KI}$ BMMs (except Poly(I:C)) (lower) are presented. n = 3. Representative results from two independent experiments. (I) Quantitative PCR analysis of TNF-α mRNA expression in BMMs stimulated with Pam3CSK4 or LPS. Average expression level in *Sh3bp2*$^{+/+}$ BMMs at 0 hour was set as 1. β-Actin was used as an endogenous control. Data are presented as means ± SEM from 3 independent experiments. (A–H) Error bars represent ± SD. *p < 0.05 vs. *Sh3bp2*$^{+/+}$ BMMs. *Tlr4*$^{del/del}$ = *TLR4*$^{lps\text{-}del/lps\text{-}del}$.

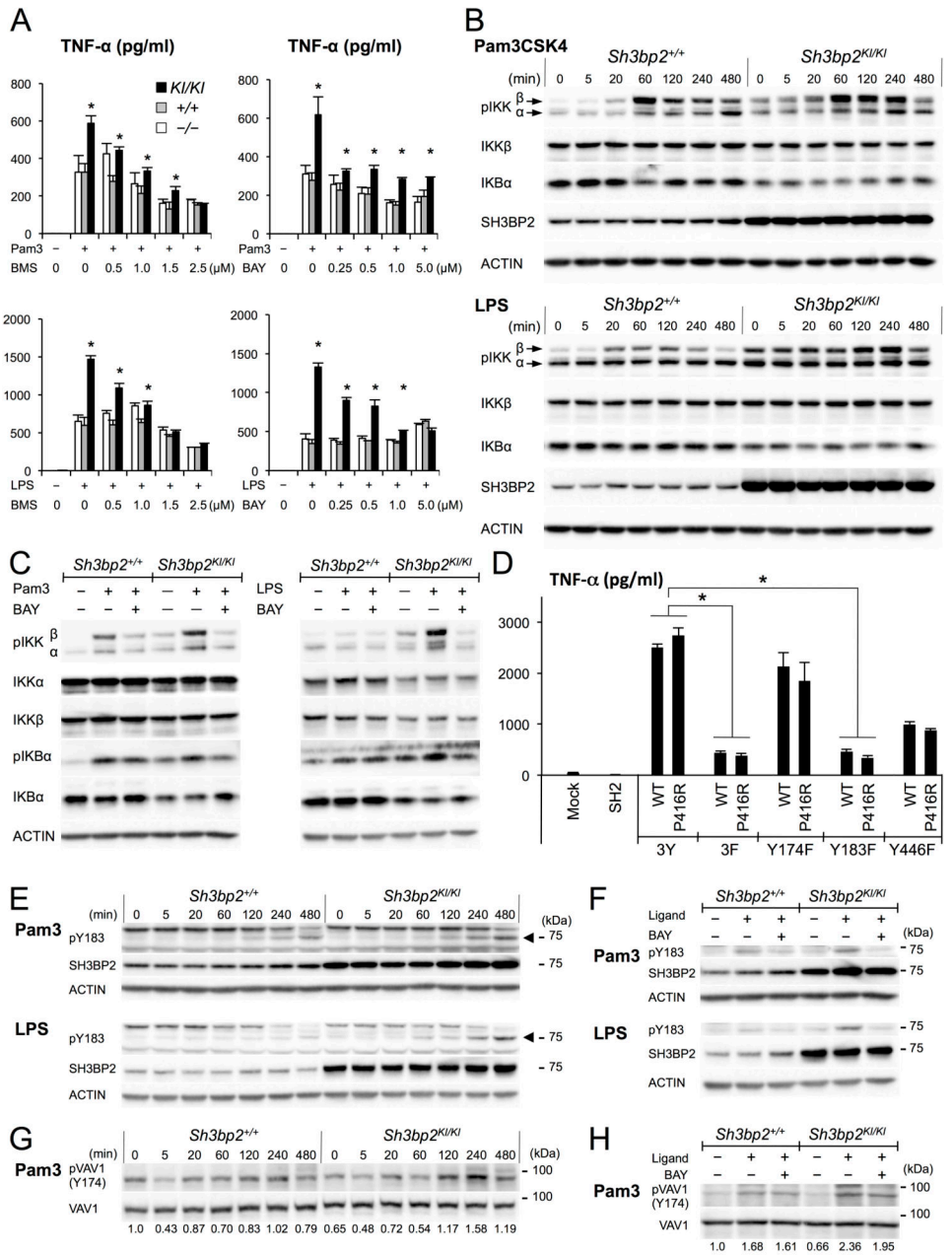

Figure 5. P416R cherubism mutation increases TNF-α production through SYK-mediated NF-κB activation

(A) Effect of IKK and SYK inhibitor on TNF-α production. BMMs were starved for M-CSF for 4–6 hours, followed by the stimulation with Pam3CSK4 or LPS for 24 hours in the presence or absence of different concentrations of BMS-345541 or BAY-613606. *$p < 0.05$ (*KI/KI* vs. +/+), n = 3. Representative results from 3 independent experiments. (B) Western blotting analysis of BMMs stimulated with Pam3CSK4 or LPS. Before stimulation BMMs were starved for serum and M-CSF for 4–6 hours. (C) Effect of SYK inhibitor (1 μM) on the activation of NF-κB pathway in the BMMs at 240 minutes after Pam3CSK4 or LPS stimulation. (D) Effect of SH3BP2 tyrosine 174, 183, and 446 residues on TNF-α

overproduction. RAW264.7 cells overexpressing wild-type (WT) or P416R mutant SH3BP2 with or without substitution of the tyrosine residues (Y) with phenylalanine (F) were seeded. Supernatants were collected after 24 hours (n = 5). SH2: C-terminal SH2-domain of SH3BP2. 3Y: Y174/183/446Y (no tyrosine substitutions). 3F: Y174/183/446F. (E) Western blotting analysis of BMMs stimulated with Pam3CSK4 or LPS with antibody against Y183-phosphorylated SH3BP2 (pY183, arrowheads) (F) Effect of BAY-613606 (1 μM) on SH3BP2 Y183 phosphorylation in BMMs at 240 minutes after Pam3CSK4 or LPS stimulation. (G) Y174 phosphorylation of VAV1 (pVAV1) after Pam3CSK4 stimulation. (H) Effect of BAY-613606 (1 μM) on VAV1 Y174 phosphorylation following Pam3CSK4 stimulation for 240 minutes. Numbers indicate relative ratio of pVAV1/total VAV1. For stimulation, 10 ng/ml of Pam3CSK4 or LPS was used. Pam3 = Pam3CSK4. BMS = BMS-345541. BAY = BAY-613606. Error bars represent ± SD. *$p < 0.05$. See also Figure S2, S3, and S4.

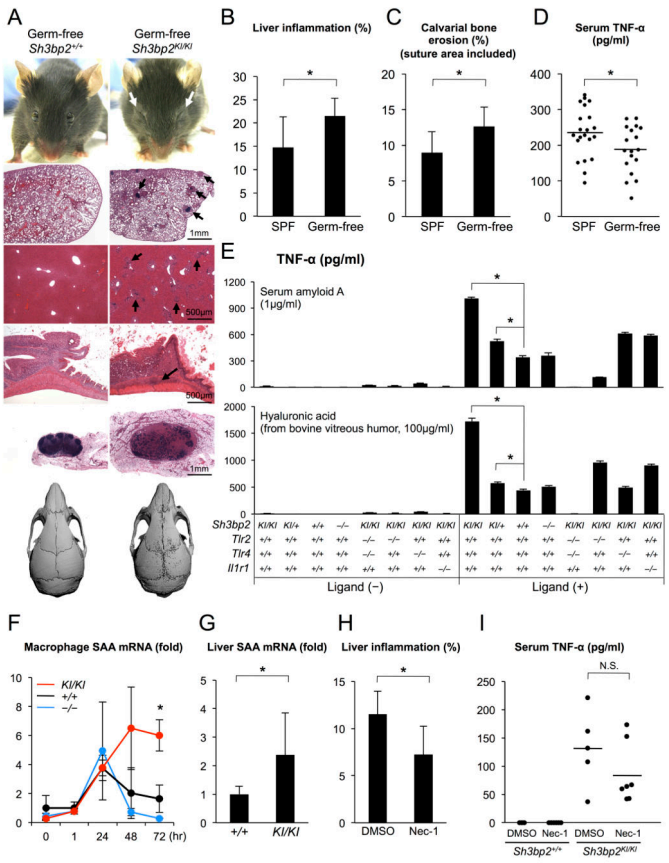

Figure 6. Microorganism-independent inflammation in *Sh3bp2*$^{KI/KI}$ mice and increased response to DAMPs in *Sh3bp2*$^{KI/KI}$ BMMs

(A) Facial appearance, H&E staining of tissues (from top: lung, liver, stomach, and lymph node), and microCT image of calvarial bone of 10-week-old germ-free *Sh3bp2*$^{+/+}$ and *Sh3bp2*$^{KI/KI}$ mice. White arrows indicate closed eyelids due to skin inflammation. Black arrows indicate inflammatory lesions. Note the development of inflammation in *Sh3bp2*$^{KI/KI}$ mice even under germ-free conditions. (B) Histomorphometric quantitation of liver inflammation in 10-week-old *Sh3bp2*$^{KI/KI}$ mice under SPF (n = 15) and germ-free (n = 19) conditions. (C) Quantitative measurement of calvarial bone erosion in 10-week-old *Sh3bp2*$^{KI/KI}$ mice under SPF (n = 11) and germ-free (n = 12) conditions. (D) Serum TNF-α levels in 10-week-old *Sh3bp2*$^{KI/KI}$ mice under SPF (n = 21) and germ-free (n = 18) conditions. (E) TNF-α levels in culture supernatants of BMMs stimulated with serum amyloid A (SAA) (1 μg/ml, top) or hyaluronic acid (100 μg/ml, bottom). (F) Quantitative PCR analysis of SAA mRNA expression in BMMs stimulated with TNF-α (10 ng/ml). Average expression level in *Sh3bp2*$^{+/+}$ macrophages before TNF-α stimulation is set as 1. Results from 3 independent experiments. (G) Quantitative PCR analysis of SAA mRNA expression in liver tissues from 3-week-old *Sh3bp2*$^{+/+}$ (n = 6) and *Sh3bp2*$^{KI/KI}$ (n = 6) mice. (H) Histomorphometric analysis of liver inflammation in 8-week-old *Sh3bp2*$^{KI/KI}$ mice injected with necrostatin-1 (Nec-1) (n = 6) or DMSO (n = 8). (I) TNF-α levels in serum of 8-week-old *Sh3bp2*$^{KI/KI}$ mice injected with Nec-1 (n = 5) or DMSO (n = 7). SPF = specific-

pathogen-free. Horizontal bars represent average. Error bars represent ± SD (B, C, E, G, H) or ± SEM (F). *p < 0.05. See also Figure S5.

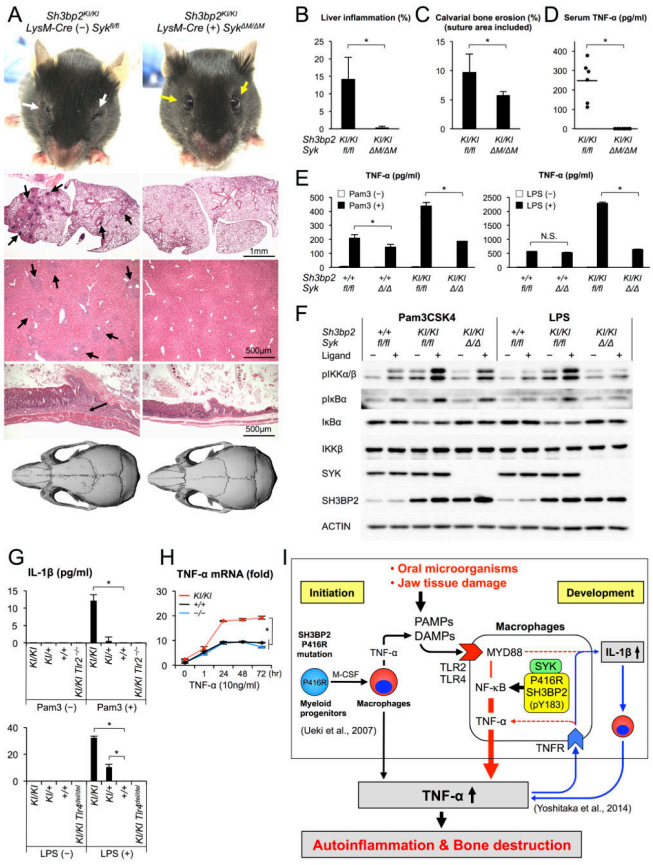

Figure 7. SYK deletion in macrophages rescues *Sh3bp2*$^{KI/KI}$ mice from inflammation and calvarial bone erosion

(A) Facial appearance, H&E staining of lung, liver, and stomach tissues, and microCT image of calvarial bone of 8-week-old *Sh3bp2*$^{KI/KI}$/*LysM-Cre* (−)/*Syk*$^{fl/fl}$ and *Sh3bp2*$^{KI/KI}$/*LysM-Cre* (+)/*Syk*$^{\Delta M/\Delta M}$ mice. Yellow arrows indicate open eyelids due to the rescue of facial skin inflammation. White arrows indicate closed eyelids due to inflamed skin. Black arrows indicate inflammatory lesions. (B) Histomorphometric analysis of liver lesions (n = 6–7). (C) Quantitative measurement of calvarial bone erosion (n = 6–7). (D) Serum TNF-α levels (*n* = 6–7). Horizontal bar represents average. (E) TNF-α levels in culture media of BMMs stimulated with Pam3CSK4 (left) or LPS (right) for 24 hours (n = 3). (F) Western blotting analysis of NF-κB pathway in Pam3CSK4- or LPS-stimulated BMMs. (G) Measurement of IL-1β levels in culture supernatants from BMMs stimulated with Pam3CSK4 or LPS (n = 3). (H) qPCR analysis of TNF-α mRNA expression in BMMs stimulated with TNF-α (10 ng/ml). Average expression level in *Sh3bp2*$^{+/+}$ BMMs at 0 hour was set as 1. Representative data from 3 independent experiments (n = 3). (I) Schematic proposal for the pathogenesis of cherubism. Mutant SH3BP2 increases myeloid cell responses not only to M-CSF (Ueki et al., 2007) for initiation of inflammation but also to TLR ligands (this study) for development of inflammation. Mutant SH3BP2 augments NF-κB activation in cooperation with SYK, resulting in the greater TNF-α production. SYK-mediated SH3BP2 phosphorylation at Y183 (pY183) plays a critical role in the process. Mutant macrophages also express more TNF-α and IL-1β in response to TNFR and TLR2/4

stimulation, respectively (dotted red lines). IL-1-mediated TNF-α inflammatory loop (blue lines) stabilizes the inflammation (Yoshitaka et al., 2014). High amounts of PAMPs and DAMPs in jaws contribute to the jaw-specific cherubism phenotype. Stabilization of jaw remodeling as well as age-dependent maturation of MYD88-independent immune system may explain the resolution of lesions after puberty in human patients. (A–D) 8-week-old mice were used for the histological and microCT comparisons. (E–G) Ten ng/ml of Pam3CSK4 or LPS was used for stimulation. Error bars represent ± SD, *$p < 0.05$. N.S.= not significant.